ELEVENTH INTERNATIONAL CONFERENCE ON INTERGRANULAR AND INTERPHASE BOUNDARIES 2004

JOURNAL OF MATERIALS SCIENCE **40** (2005) 3247–3254

Reactions of slip dislocations with twin boundary in Fe-Si bicrystals

A. GEMPERLE, N. ZÁRUBOVÁ*, J. GEMPERLOVÁ
Institute of Physics ASCR, Na Slovance 2, CZ-182 21 Praha 8
E-mail: zarubova@fzu.cz

Specimens for *in situ* TEM straining were prepared from Fe-5.5 at.%Si $\Sigma 3$ bicrystals with {112} grain boundary plane. They were strained under three different directions of the stress at the boundary with respect to the orientation of the grains. Transfer of slip across the boundary was analysed. In one case, the transfer of slip was realized by a transformation of the slip dislocation in one grain into the slip dislocation in the other grain. Low energy dislocation was created in the GB in accordance with general transfer criteria. In the second case, the incoming and outgoing slip systems were in direct contraction to the general transfer criteria. In the third case, oriented for common slip system in both grains, the trapped incoming slip dislocations dissociated into twinning dislocations which created twins on the other side of the boundary.

1. Introduction

A simple geometric and stress criterion for the transmission of dislocations across a high angle grain boundary (GB) was suggested by Shen *et al*. [1]. Lee *et al*. [2, 3] added two further conditions. The conditions for the slip transfer may be summarized as follows. The angle α between the lines of intersection of the incoming and outgoing slip planes with the GB should be minimal as well as the angle β between the Burgers vectors of the incoming and outgoing dislocations. This condition is commonly expressed by the factor $M = \cos\alpha \cos\beta$ that should be maximal. The resolved shear stress of the possible slip system in the adjoining grain should be large. The magnitude of the Burgers vector of the residual dislocation left in the GB after the transfer should be a minimum.

Following these criteria, the easiest propagation would involve dislocations having the Burgers vector common in both grains and moving in planes that have a common intersection with the interface. This was confirmed by X-ray topography and electron microscopy observation of Si and Ge [4, 5]. In bcc bicrystals, an analogous case is a slip transmission across a symmetric {1 1 2} GB for common (110) slip plane and common $\frac{1}{2}[\bar{1}\,1\,1]_A = \frac{1}{2}[\bar{1}\,1\,\bar{1}]_B$ Burgers vectors of slip dislocations in adjoining grains A and B. However, experiments using white-beam synchrotron radiation topography on Fe-Si alloys [6] showed that in the case of symmetric $\Sigma 3$ bicrystals the direct slip transfer is difficult.

Gemperlová *et al*. [7] performed both *in situ* straining and post mortem TEM experiments on symmetric $\Sigma 3$ bicrystals. They found that slip dislocations with the Burgers vector $\frac{1}{2}[\bar{1}\,1\,1]_A$ lying in the boundary plane $(\bar{1}\,1\,\bar{2})_A$ are trapped in the boundary and dissociate into three GB dislocations $\frac{1}{6}[\bar{1}\,1\,1]_A$. The dissociation is accompanied by a large reduction of energy. This prevents the dislocations from passing freely the GB. However, the direct transmission was observed for slip system $\frac{1}{2}[1\,1\,1]_B/(0\,1\,\bar{1})_B$ into $\frac{1}{2}[1\,1\,1]_A/(\bar{5}\,7\,\bar{2})_A$. Two $\frac{1}{6}[\bar{1}\,1\,1]_A$low energy residual dislocations were left in the boundary.

In the experiments presented here, specimens with modified tensile axis orientations have been used. The transfer of slip across GB is examined and the criteria of slip transfer are discussed.

2. Experimental

The experiments were carried out on $\Sigma 3$ twin bicrystals 70.5° / [1 1 0], with $(\bar{1}\,1\,\bar{2})_A = (1\,\bar{1}\,\bar{2})_B$ GB plane. Two bicrystals of Fe-5.5 at%Si , with a very low dislocation density, were grown by floating zone melting in the Institute of Physics ASCR. Tensile samples $1.7 \times 5.5 \times 0.1$ mm^3 were prepared from the bicrystals by oriented spark-cutting and mechanical grinding. A small hole in the specimen centre was made in a modified Fischione double jet polisher. Special care was taken so that the GB passes the hole tangentially (Fig. 1). The crystallographic orientations of the specimens are given in Figs 2, 7, 12 and Table I.

The samples were tensile strained at room temperature in a JEM 1200EX microscope. An improved double tilt straining stage was constructed in the Institute of Physics ASCR [8]. The estimated specimen cross-section in the thinnest part is 0.06 to 0.08 mm^2. The critical resolved shear stress of Fe-5.5 at%Si is 128 MPa [9]. Thus, the load necessary to start plastic deformation

*Author to whom all correspondence should be addressed.

TABLE I Analysis of slip transfer. The slip system is characterised by Burgers vector/slip plane, μ is the Schmid factor, $M = \cos\alpha \cos\beta$, $\mathbf{b}_{res}$ is the Burgers vectors of residual dislocation, $\mathbf{b}_{GBD}$ is the Burgers vector of GB dislocation, the energy of a residual dislocation is proportional to b^2, dissociation $\mathbf{b}_{res}$ into $\mathbf{b}_{GBD}$ reduces its value

*S*1 foil normal $[\bar{3}\,2\,\bar{1}]_A = [\bar{2}\,\bar{1}\,\overline{11}]_B$
load axis σ $[3\,5\,1]_A = [3\,5\,\bar{1}]_B$, actual tensile axis σ_L $[3\,5\,1]_A = [3\,5\,\bar{1}]_B$

MRSS slip system in grain A: $\frac{1}{2}[11\bar{1}]_A/(1\,4\,5)_A$, $\mu = 0.499$
Active slip system in grain A $\frac{1}{2}[1\,1\,1]_A/(0\,1\,\bar{1})_A$, $\mu = 0.420$

Slip systems in B	μ	M	$\mathbf{b}_{res}$	$\mathbf{b}_{GBD}$	$\mathbf{b}^2_{res} \rightarrow \Sigma\mathbf{b}^2_{GBD}$
$\frac{1}{2}[1\,1\,1]_B/(1\,4\,\bar{5})_B$	0.499	0.473	$\frac{1}{6}[\bar{2}\,2\,2]_A = \frac{1}{6}[\bar{2}\,2\,\bar{2}]_B$	$\mathbf{2b}_S$	$0.334 \rightarrow 0.167$
$\frac{1}{2}[\bar{1}\,1\,1]_B/(5\,7\,\bar{2})_B$	0.097	0.536	$\frac{1}{3}[1\,2\,\bar{1}]_A = \frac{1}{3}[2\,1\,\bar{1}]_B$	**b**	0.667
$\frac{1}{2}[\bar{1}\,1\,\bar{1}]_B/(1\,1\,0)_B$	0.280	0.333	$[1\,0\,0]_A = \frac{1}{3}[2\,1\,2]_B$		1.000
$\frac{1}{2}[1\,1\,\bar{1}]_B/(0\,1\,1)_B$	0.420	0.556	$\frac{1}{3}[1\,\bar{1}\,2]_A = \frac{1}{3}[\bar{1}\,1\,2]_B$	**b**	0.667

*S*2 foil normal $[\overline{17}\,\bar{1}\,\bar{4}]_A = [\bar{3}\,\bar{3}\,\bar{4}]_B$,
load axis σ $[\bar{1}\,5\,3]_A = [\bar{1}\,5\,\bar{3}]_B$, actual tensile axis $\sigma_L[\bar{3}\,23\,7]_A = [1\,19\,\overline{15}]_B$

MRSS slip system in grain A $\frac{1}{2}[1\,1\,1]_A/(\bar{6}\,7\,\bar{1})_A$, $\mu = 0.492$
Active slip system in grain A $\frac{1}{2}[1\,1\,1]_A/(\bar{6}\,7\,\bar{1})_A$, $\mu = 0.492$

Slip systems in B	μ	M	$\mathbf{b}_{res}$	$\mathbf{b}_{GBD}$	$\mathbf{b}^2_{res} \rightarrow \Sigma\mathbf{b}^2_{GBD}$
$\frac{1}{2}[1\,1\,1]_B/(\bar{1}\,24\,\overline{23})_B$	0.118	0.707	$\frac{1}{6}[\bar{2}\,2\,2]_A = \frac{1}{6}[\bar{2}\,2\,\bar{2}]_B$	$\mathbf{2b}_S$	$0.334 \rightarrow 0.167$
$\frac{1}{2}[\bar{1}\,1\,1]_B/(1\,9\,\bar{8})_B$	0.071	0.473	$\frac{1}{3}[1\,2\,\bar{1}]_A = \frac{1}{3}[2\,1\,\bar{1}]_B$	**b**	0.667
$\frac{1}{2}[\bar{1}\,1\,\bar{1}]_B/(3\,2\,\bar{1})_B$	0.486	0.034	$[1\,0\,0]_A = \frac{1}{3}[2\,1\,2]_B$		1.000
$\frac{1}{2}[1\,1\,\bar{1}]_B/(\overline{13}\,9\,\bar{4})_B$	0.460	0.533	$\frac{1}{3}[1\,\bar{1}\,2]_A = \frac{1}{3}[\bar{1}\,1\,2]_B$	**b**	0.667

*S*3 foil normal $[\bar{3}\,2\,\bar{1}]_A = [\bar{2}\,\bar{1}\,\overline{11}]_B$
load axis σ $[3\,5\,1]_A = [3\,5\,\bar{1}]_B$, actual tensile axis $\sigma_L[0\,1\,2]_A = [\bar{1}\,2\,0]_B$

MRSS slip system in grain A $\frac{1}{2}[1\,1\,1]_A/(\bar{1}\,0\,1)_A$ and $\frac{1}{2}[\bar{1}\,1\,1]_A/(1\,0\,1)_A$, $\mu = 0.490$,
Active slip system in grain A $\frac{1}{2}[\bar{1}\,1\,1]_A/(1\,0\,1)_A$

Slip systems in B	μ	M	$\mathbf{b}_{res}$	$\mathbf{b}_{GBD}$	$\mathbf{b}^2_{res} \rightarrow \Sigma\mathbf{b}^2_{GBD}$
$\frac{1}{2}[1\,1\,1]_B/(\bar{4}\,5\,\bar{1})_B$	0.245	0.040	$\frac{1}{3}[\bar{4}\,1\,1]_A = [\bar{1}\,0\,\bar{1}]_B$		2.000
$\frac{1}{2}[\bar{1}\,1\,1]_B/(0\,1\,\bar{1})_B$	0.490	0.174	$\frac{1}{3}[\bar{2}\,2\,\bar{1}]_A = [0\,0\,\bar{1}]_B$		1.000
$\frac{1}{2}[\bar{1}\,1\,\bar{1}]_B/(0\,1\,1)_B$	0.490	1.000	0		0.000
$\frac{1}{2}[1\,1\,\bar{1}]_B/(\bar{4}\,5\,1)_B$	0.245	0.050	$\frac{1}{3}[\bar{2}\,\bar{1}\,2]_A = [\bar{1}\,0\,0]_B$		1.000

$\mathbf{b} = \frac{1}{3}\,\langle 1\,1\,2\rangle_{A,B}$, $\mathbf{b}_S = \frac{1}{6}\,\langle 1\,1\,1\rangle_{A,B}$.

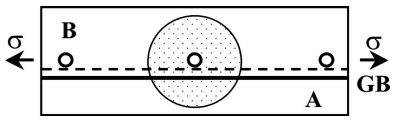

Figure 1 Specimen shape. GB trace at upper surface is denoted by thick line, dashed line—GB trace at lower surface. σ is load axis. Depression area is dotted.

on a slip system with the maximum Schmid factor 0.5 is about 18 N. In the previous experiments performed at CEA and UJF, Grenoble, the available load was only 10 N. Therefore only substantially thinner Fe-Si samples with lower Si content could be deformed in the transparent area. The new holder was designed with 25 N maximum load. Moreover, an enlarged y-tilt of $\pm 10^\circ$ independent of the x-tilt provided by the new straining stage ensures good imaging conditions.

The specimens were observed during straining under two-beam bright field conditions using different reflections in the two grains. The observations were registered by MegaView III camera. A detailed *post mortem* analysis of the dislocation structure, active Burgers vectors and corresponding slip planes was made using two-beam bright and dark field conditions in various reflections.

3. Results

3.1. Active slip systems

In the present *in situ* straining experiments, the local stress distribution in the foil was considerably modified by the presence of the hole and the observed slip systems did not necessarily correspond to the predicted ones. Different slip systems could be thus activated in foils of the same orientation as illustrated below. In order to use meaningfully the slip transfer criteria, the active slip systems were determined and the actual tensile axes were reconstructed from observed slip traces on the foil surface and the active slip vectors. The Burgers vector of the dislocations was found using the **g.b** criteria. The actual (local) direction of the tensile stress, σ_L, was determined based on the following premise. The slip plane of $\frac{1}{2}\,\langle 1\,1\,1\rangle$ is the maximum resolved shear stress (MRSS) plane [10]. Therefore σ_L lies in the plane given by the slip vector and the normal of the slip plane. The σ_L is parallel to the foil surface. In the proximity of GB, the directions of σ_L determined independently in either grain must be very close.

3.2. TEM observations

3.2.1. Specimen S1

Orientation of the sample during straining is shown in Fig. 2. A frame of the video record of the straining experiment is reproduced in Fig. 3. Slip started in grain A and continued in grain B. The slip systems were identified as $\frac{1}{2}[1\,1\,1]_A/(01\bar{1})_A$ and $\frac{1}{2}[1\,1\,1]_B/(14\bar{5})_B$. The GB is outside the hole in this case, therefore the direction of the tensile stress remained unchanged. An edge of the area of slip transfer from grain A to grain B is visible in the centre of Fig. 4 where slip traces in both grains are imaged. The slip traces in grain B have rather diffuse contrast. In the area of the boundary, the distinct lines approximately along $[\bar{1}\,1\,1]_A$ are trapped dislocations

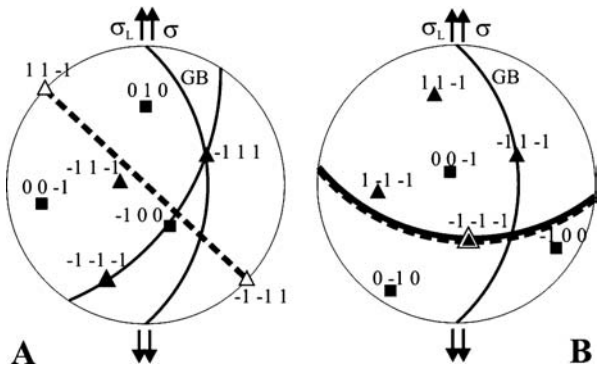

Figure 2 Stereographic projections of grains A and B in the foil. σ, σ_L are directions of the load axis and the actual tensile stress, respectively. –△– are predicted slip systems $[11\bar{1}]_A/(1\,4\,5)_A$ and $[1\,1\,1]_B/(1\,4\,\bar{5})_B$. —▲— are active slip systems $[1\,1\,1]_A/(01\bar{1})_A$ and $[1\,1\,1]_B/(1\,4\,\bar{5})_B$.

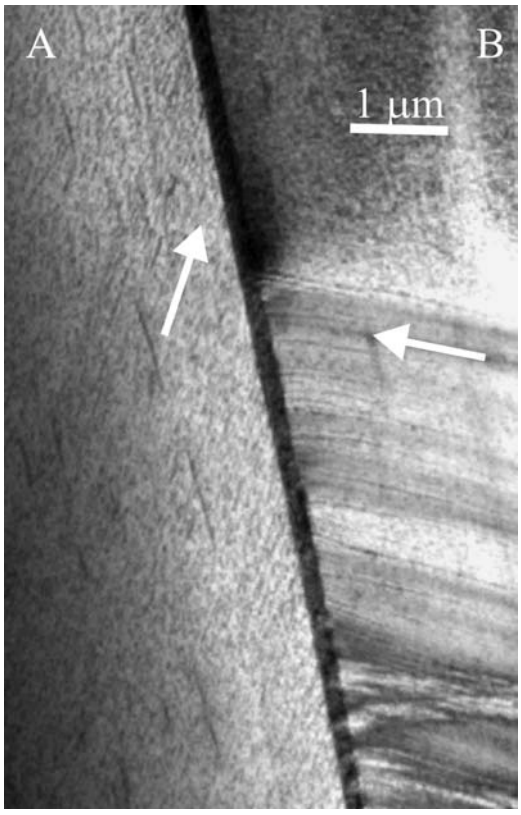

Figure 3 A frame of video record. Direction of slip traces in both grains marked by arrows.

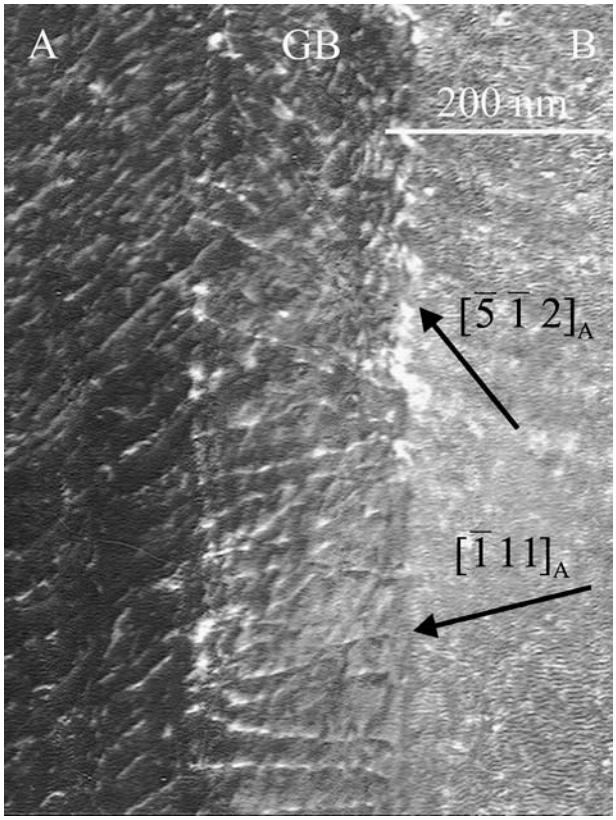

Figure 4 Edge of the area of slip transfer from grain A to grain B visible in the image centre. Trapped slip dislocations $\frac{1}{2}[111]_A$ are marked by arrows. DF 110_{AB}.

$\frac{1}{2}[1\,1\,1]_A$. At the edge of the transfer area, the $\frac{1}{2}[1\,1\,1]_A$ slip dislocations are gradually rotated in the boundary from the direction $[\bar{1}\,1\,1]_A$ towards $[\bar{5}\,\bar{1}\,2]_A$. The inner part of the slip transfer area is shown in Fig. 5a. The straight lines along $[\bar{5}\,\bar{1}\,2]_A$ directions are evidently residual dislocations $\frac{1}{3}[\bar{1}\,1\,1]_A$ and wavy lines along $[\bar{1}\,1\,1]_A$ direction are trapped slip dislocations. The slip traces in grain B are much more pronounced than in Fig. 4. Slip dislocations $\frac{1}{2}[1\,1\,1]_B$ are visible at the ends of some slip traces in Fig. 5b. The residual dislocations are best visible in Fig. 6. The dense regular array of parallel dislocations along $[1\,7\,\bar{3}]_B$ are intrinsic tilt dislocations $\frac{1}{3}[1\,\bar{1}\,\bar{2}]_B$ compensating a deviation from the exact coincidence.

3.2.2. Specimen S2

Orientation of the sample during straining is shown in Fig. 7. Two frames of the video record of the straining experiment are reproduced in Fig. 8. Slip started in grain A at about 18 N (Fig. 8a) and transferred to grain B after a load increase (Fig. 8b). The active slip systems in grain A and B were identified as $[111]_A/(\bar{6}7\bar{1})_A$ and $[\bar{1}1\bar{1}]_B/(32\bar{1})_B$, respectively. The actual tensile axis σ_L was inclined by 15° to the load axis (Fig. 7). The post mortem analysis of the dislocation structure concentrated on the area where slip traces were observed on either side of the boundary on the video record. In Fig. 9 slip dislocations $\frac{1}{2}[1\,1\,1]_A = \frac{1}{6}[1\,5\,1]_B$ trapped in the boundary are visible as nearly straight lines in $[\bar{8}\,\bar{7}1]_A$ direction. Slip dislocations $\frac{1}{2}[\bar{1}\,1\,\bar{1}]_B$ of grain

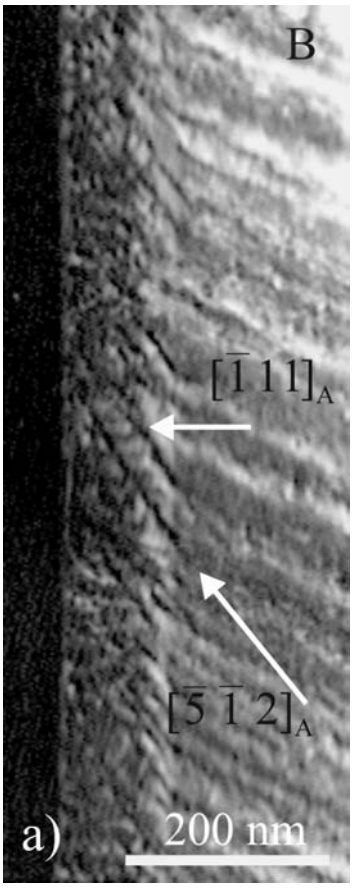

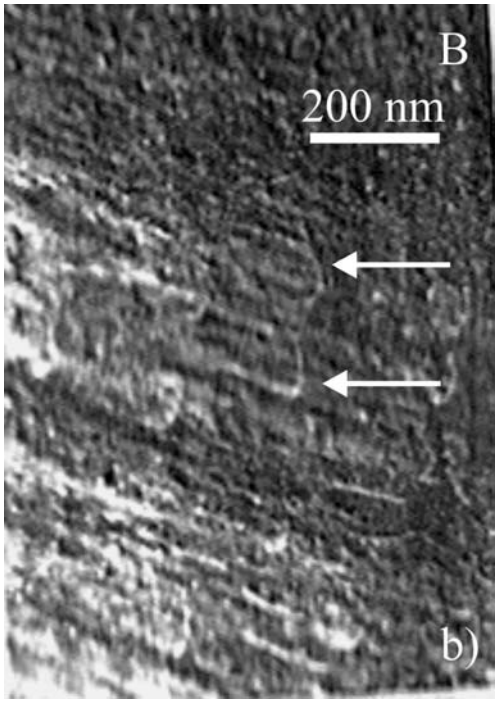

Figure 5 (a) Inner part of slip transfer area. Trapped slip $\frac{1}{2}[111]_A$ dislocations lie along $[\bar{1}11]_A$ direction, residual $\frac{1}{3}[\bar{1}11]_A$ dislocations along $[\bar{5}\bar{1}2]_A$. (b) Slip dislocations $\frac{1}{2}[111]_B$ visible at the ends of slip traces in grain A (see arrows). DF 020_B.

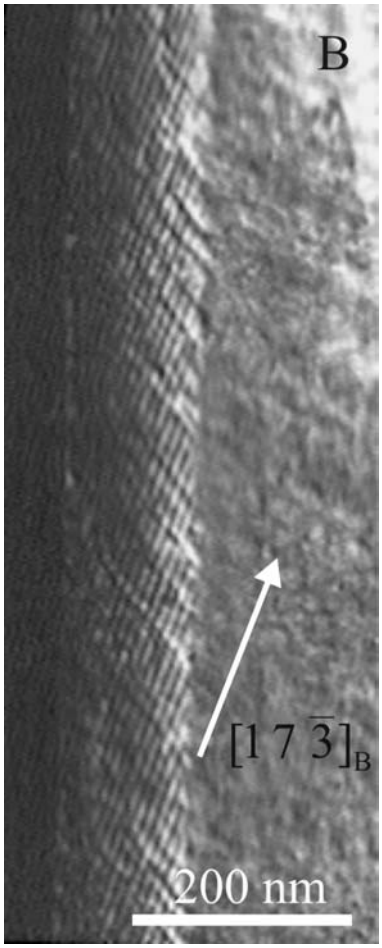

Figure 6 Inner part of slip transfer area. The residual dislocations are well visible. The dense array of parallel dislocations along $[1\,7\,\bar{3}]_B$ are intrinsic tilt dislocations $\frac{1}{3}[1\bar{1}\bar{2}]_B$. DF $\bar{1}10_B$.

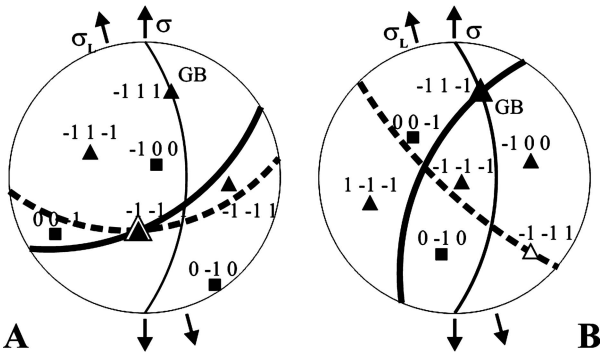

Figure 7 Stereographic projections of grains A and B in the foil. σ, σ_L are directions of the load axis and the actual tensile stress, respectively. –△– are predicted slip systems $[1\,1\,1]_A/(\bar{5}\,4\,1)_A$ and $[1\,1\,\bar{1}]_B/(\bar{5}\,4\,\bar{1})_B$. —▲— are active slip systems $[1\,1\,1]_A/(\bar{6}\,7\,\bar{1})_A$ and $[\bar{1}\,1\,\bar{1}]_B/(3\,2\,\bar{1})_B$.

B, with $\mathbf{gb} = 1$, are present neither in the boundary nor in grain B near the boundary. The same area is imaged in Fig. 10. Slip dislocations $\frac{1}{2}[1\,1\,1]_A$ are weakly visible. Beside them, dislocations of moderate density bowed in the boundary between the intersections with the two foil surfaces show also a distinct contrast. They are better visible in Fig. 10. Both types of dislocations namely, slip dislocations $\frac{1}{2}[1\,1\,1]_A$ and the bowed dislocations are in Fig. 11. The regular dense array of parallel dislocations represents intrinsic tilt GB dislocations $\frac{1}{3}[\bar{1}\,1\bar{2}]_A$.

3.2.3. Specimen S3

The crystallographic orientation of the foil (Fig. 12) was identical with that of the sample *S*1 (Fig. 2). Slip

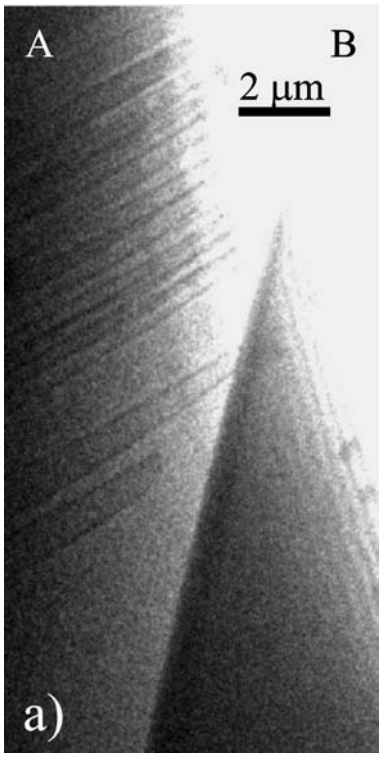

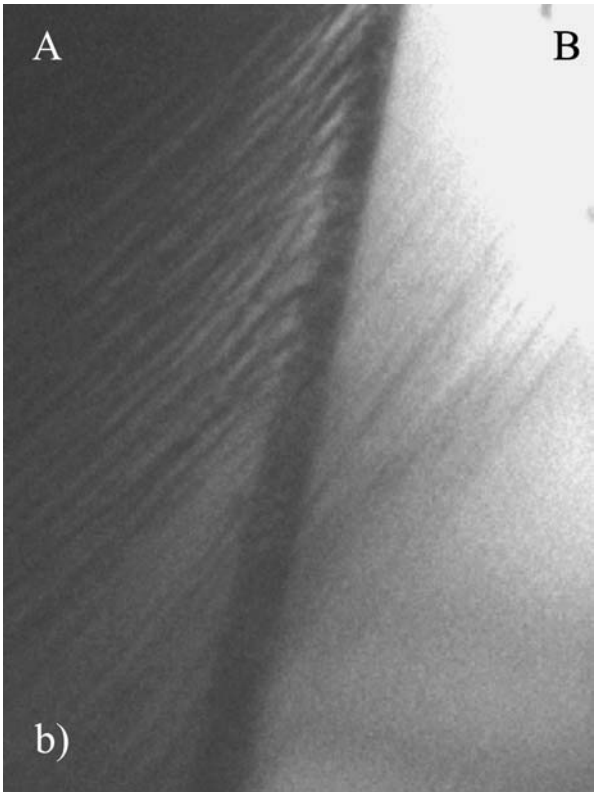

Figure 8 Two frames of video record. (a) Early stage of deformation. Slip traces visible only in grain A. (b) Later stage of deformation. Slip traces visible in both grains.

started in grain A at a load of 20 N. The slip bands reached the GB, and after an increment of the load to 22 N, discrete twins appeared in the adjoining grain B (Fig. 13). The slip system in grain A was identified as $[\bar{1}11]_A/(101)_A$. The direction of the actual tensile stress was strongly turned in this case (Fig. 12). The MRSS plane in grain B was $(011)_B$, parallel to $(101)_A$. In the vicinity of the GB, however, no slip on the $(011)_B$ plane

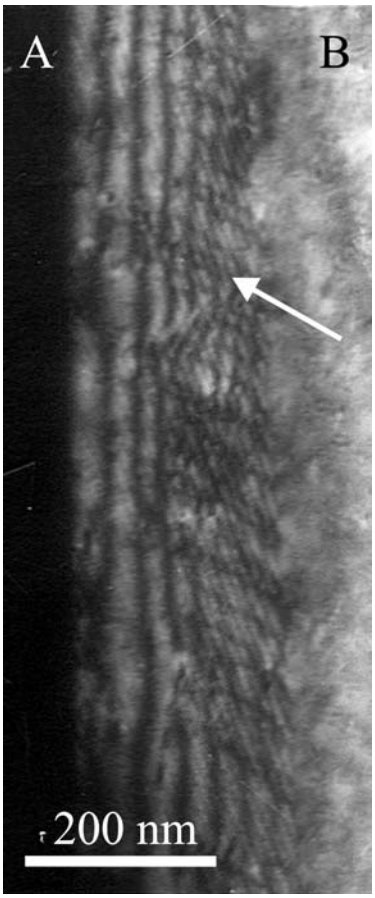

Figure 9 Slip dislocations $\frac{1}{2}[1\,1\,1]_A$ trapped in the boundary visible as nearly straight lines (see arrow). DF $1\,\bar{1}\,0_B$.

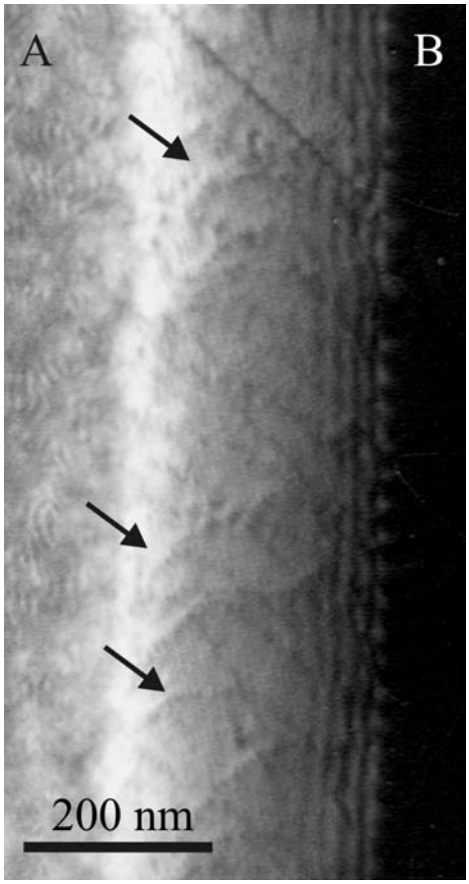

Figure 10 Bowed dislocations in the boundary (see arrows) visible with distinct contrast. Slip dislocations trapped in the GB weakly visible. DF $01\bar{1}_A$.

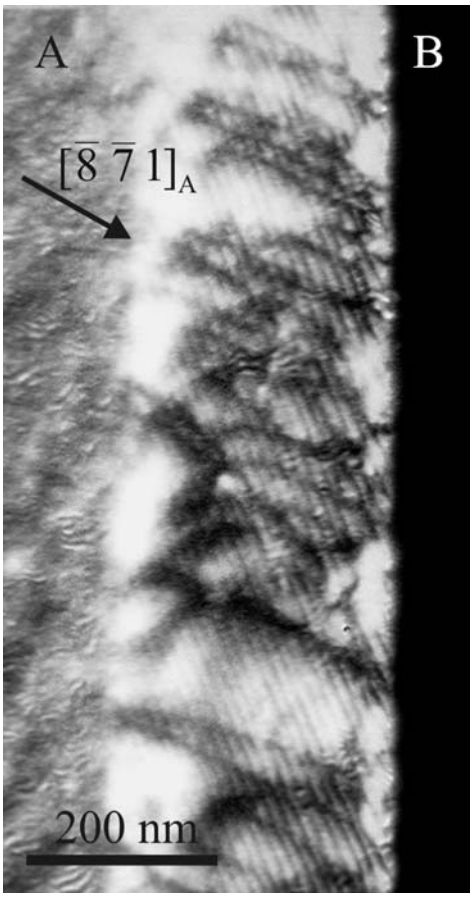

Figure 11 Slip dislocations and bowed dislocations with distinct dark contrast. Regular dense array of parallel dislocations are intrinsic tilt dislocations $\frac{1}{3}[\bar{1}1\bar{2}]_A$. DF 020_A.

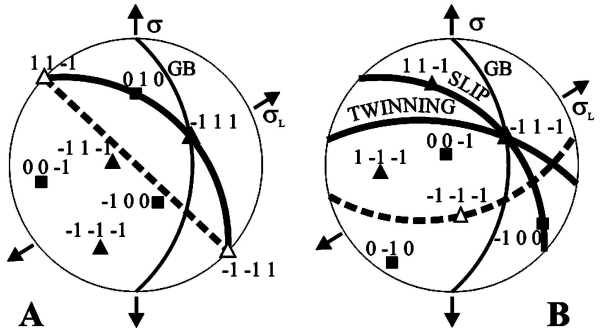

Figure 12 Stereographic projections of grains A and B in the foil. σ, σ_L are directions of the load axis and the actual tensile stress, respectively. –△– are predicted slip systems $[11\bar{1}]_A/(1\,4\,5)_A$ and $[111]_B/(1\,4\,\bar{5})_B$. —▲— are active slip systems $[\bar{1}11]_A/(101)_A$ and $[\bar{1}1\bar{1}]_B/(011)_B$, and twinning system $[\bar{1}1\bar{1}]_B/(12\,1)_B$.

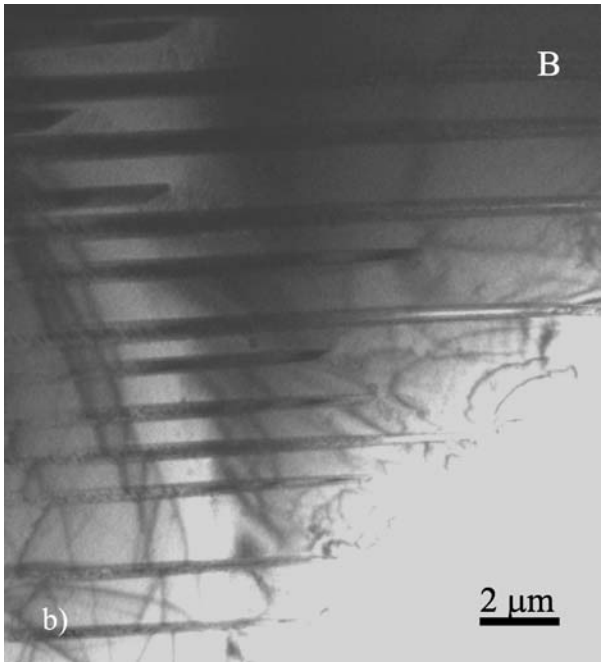

Figure 13 Frames of video record. (a) Traces of slip dislocations in grain A. (b) Overall view of twins in grain B.

was detected. Instead twins appeared in grain B having the habit plane $(121)_B$. Their intersection with the GB is shown in Fig. 14. Twinning dislocations of weak contrast are visible in the twins near the intersection. The same twins imaged farther from the GB are shown in Fig. 15. Twinning dislocations in the coherent boundary are visible with good contrast. The Burgers vector of twinning dislocations is $\frac{1}{6}[\bar{1}1\bar{1}]_B$. The twins have the same crystallographic orientation as grain A. In Fig. 16 twin tips emit $\frac{1}{2}[\bar{1}1\bar{1}]_B$ slip dislocations which move on actual MRSS planes $(011)_B$ and relieve the stresses due to tips.

4. Discussion

The experiment *S*1 (Figs 2–6) involves transformation of $\frac{1}{2}[1\,1\,1]_A$ into $\frac{1}{2}[1\,1\,1]_B$ dislocations. This transformation produces $\frac{1}{6}[\bar{2}\,2\,2]_A = \frac{1}{6}[\bar{2}\,2\,\bar{2}]_B$ residual dislocations which decompose spontaneously in two equal low energy GB dislocations (Table I). The other possible transformation to $\frac{1}{2}[1\,1\,\bar{1}]_B$ has by 15% higher M and by 16% lower Schmid factor. However, the decisive role in such a case is attributed to the energy of the residual dislocations, as stressed by Lee *et al*. [3]. It is four times lower for the first transformation. The contrast of the residual dislocations is compatible with $[\bar{1}\,1\,1]_A$ Burgers vector direction.

The experiment *S*1 is analogical to the experiment described in the paper [7]. In both cases the slip

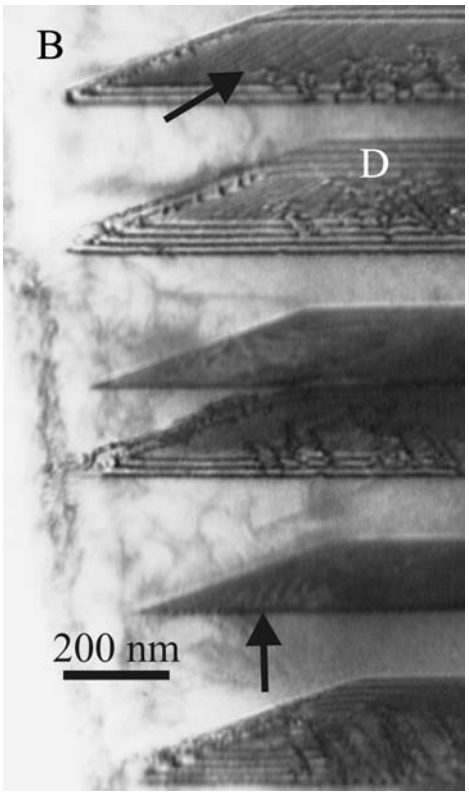

Figure 14 Deformation twins in grain B emerging from the GB (on the left). Twinning dislocations–see arrows. The twins contain many defects (D). BF $1\bar{2}\bar{3}_A$.

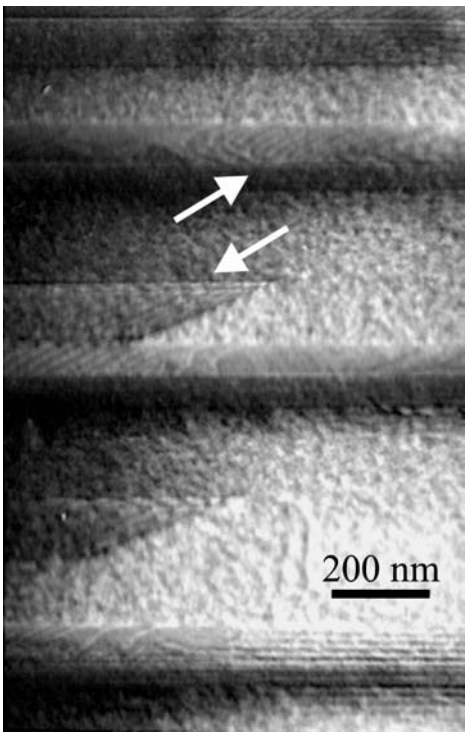

Figure 15 The same twins as in Fig. 14, farther from the GB. Twinning dislocations in the coherent boundary—see arrows. DF $\bar{1}10_B$.

transfer involves mutual transformation of $\frac{1}{2}[1\,1\,1]_A$ and $\frac{1}{2}[1\,1\,1]_B$ dislocations. The difference between the two cases is in the final residual dislocation configuration in the boundary. In the transfer from B to A [7] the incoming dislocation has to rotate from its slip plane by 22° towards in the sense $[\bar{1}\,1\,\bar{1}]_B$. The residual dislocations evidently continue to rotate in the same sense by

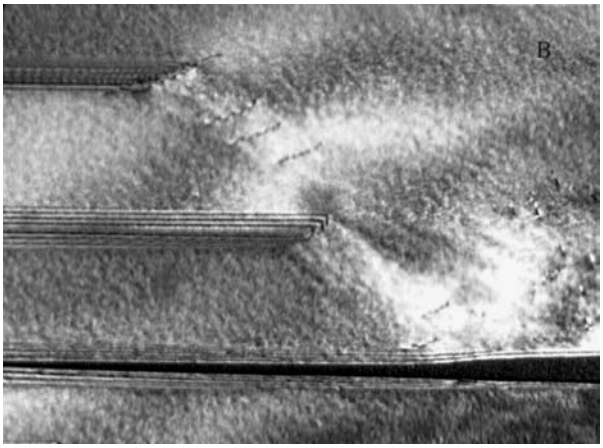

Figure 16 Twin tips emitting $\frac{1}{2}[\bar{1}1\bar{1}]_B$ slip dislocations. DF $\bar{1}10_B$.

further 32° and take the screw orientation. In the transfer from A to B (present case *S*1) the A dislocation has to rotate from its slip plane by 43° in the sense from $[\bar{1}\,1\,1]_A$. The residual dislocation would have to rotate back by the same angle to take the low energy screw orientation. This is evidently not possible. Therefore the present transformation has higher energy and needs probably also a higher stress.

In the experiment *S*2 (Figs 7–11) the A grain deforms by the same slip system as in *S*1. The transfer of slip via the $\frac{1}{2}[1\,1\,1]_B$ vector is excluded in this case by the very low Schmid factor (Table I). Considering the transfer criteria, slip vector $\frac{1}{2}[1\,1\,\bar{1}]_B$ is the best choice. It has the second highest Schmid factor, only by 5% lower than slip vector $\frac{1}{2}[\bar{1}\,1\,\bar{1}]_B$, and reasonably high M factor. The residual dislocation is a GB dislocation, though of a rather high energy. Slip vector $\frac{1}{2}[\bar{1}\,1\,\bar{1}]_B$ has a very low M factor. Its residual dislocation is not a GB dislocation and has even higher energy than that of $\frac{1}{2}[1\,1\,\bar{1}]_B$. However, slip trace observation in reflections $10\bar{1}_B$, $1\bar{1}0_B$ and $01\bar{1}_B$ eliminated the vector $\frac{1}{2}[1\,1\,\bar{1}]_B$ and decided in favour of $\frac{1}{2}[\bar{1}\,1\,\bar{1}]_B$. No residual dislocations were detected in the boundary. The transfer of slip by the slip system $\frac{1}{2}[\bar{1}\,1\,\bar{1}]_B/(32\bar{1})_B$ is in direct contradiction to the transfer criteria.

The possibility of dislocation sources activated in grain B can be excluded by the absence of B dislocations in the boundary and close by it. A close examination of Fig. 10 reveals that some bowed segments of dislocations in the boundary are clearly linked up with straight segments of trapped $\frac{1}{2}[1\,1\,1]_A$ dislocations. This indicates a rearrangement of the $\frac{1}{2}[1\,1\,1]_A$ dislocations in the boundary with the result that parts of them are rotated towards the direction of intersection of $(32\bar{1})_B$ slip plane with the boundary. Some mechanism of slip transfer initiated in the boundary is therefore probable. However, its nature could not be explained and is surely worth further analysis.

The experiment *S*3 (Figs 12–16) represents the theoretical easy slip configuration with $\frac{1}{2}[\bar{1}\,1\,1]_A$, $\frac{1}{2}[\bar{1}\,1\,\bar{1}]_B$ common Burgers vectors and $(\bar{1}01)_A$, $(011)_B$ common slip planes (Table I). It was shown in [7] that the slip transfer on these systems is impeded by the dissociation of incoming $\frac{1}{2}$ <1 1 1> slip dislocations into

three $\frac{1}{6}$ <1 1 1> GB dislocations. The $\frac{1}{6}[\bar{1}\,1\,1]_A$ dislocations trapped in the boundary are twinning dislocations $\frac{1}{6}[\bar{1}\,1\,\bar{1}]_B$. At a sufficiently large stress they leave the boundary moving on $(121)_B$ neighbouring planes and create $70.5°/[10\bar{1}]_B$, $(121)_B$ twins. It may be easily verified that the crystallographic orientation of these twins is identical to the orientation of grain A. The additional stresses at the tips of the twins (Fig. 16) are high enough to enable the combination of three $\frac{1}{6}[\bar{1}\,1\,\bar{1}]_B$ twinning dislocations into a $\frac{1}{2}[\bar{1}\,1\,\bar{1}]_B$ slip dislocation that moves on $(011)_B$ MRSS plane and relieves the additional stress. The recombination of $\frac{1}{2}[\bar{1}\,1\,\bar{1}]_B$ dislocations at the tip of a twin is evidently easier than their recombination in the GB. The observed transfer of deformation across the GB by twinning is another new effect not predicted by the earlier formulated slip transfer criteria.

5. Conclusions

Three *in situ* straining experiments involving slip transfer across a coherent twin boundary in Fe-5.5 at.%Si bicrystal were performed. They differ by the orientation of the direction of stress at the boundary with respect to the orientation of the lattice in the grains. The results were compared with the transfer criteria formulated earlier. In the first case the transfer of slip was compatible with them. In the second case the results of analysis realized as yet are in direct contradiction to the transfer criteria. In the third case the deformation was transferred by twinning instead of the expected easy slip. It is obvious that the mechanisms of slip transfer across grain boundaries are more complex than it was believed and they need further study.

Acknowledgement

Authors highly acknowledge financial support of GA CR (Contracts 202/01/0670 and 202/04/2016).

References

1. Z. SHEN, R. H. WAGONER and W. A. T. CLARK, *Scripta Metall.* **20** (1986) 921.
2. T. C. LEE, I. M. ROBERTSON and H. K. BIRNBAUM, *ibid.* **23** (1989) 799.
3. *Idem.*, *Phil. Mag. A* **62** (1990) 131.
4. X. BAILLIN, J. PELISSIER, A. JACQUES and A. GEORGES, *ibid.* **61** (1990) 329.
5. A. JACQUES, A. GEORGE, X. BAILLIN and J. J. BACMANN, *ibid.* **55** (1987) 165.
6. M. POLCAROVÁ, J. GEMPERLOVÁ, J. BRÁDLER, A. JACQUES, A. GEORGE and L. PRIESTER, *ibid.* **78** (1998) 105.
7. J. GEMPERLOVÁ, A. JACQUES, A. GEMPERLE and N. ZÁRUBOVÁ, *Interf. Sci.* **10** (2002) 51.
8. Z. DLABÁČEK, A. GEMPERLE and J. GEMPERLOVÁ, *Proc. EMC 2004*, Antwerp (2004).
9. V. NOVÁK, K. Z. SALEEB, S. KADEČKOVÁ and B. ŠESTÁK, *Czech. J. Phys. B* **26** (1976) 565.
10. B. ŠESTÁK and N. ZÁRUBOVÁ, *Phys. Stat. Sol.* **10** (1965) 239.

Received 15 September 2004
and accepted 31 January 2005